PROCEEDINGS OF SPIE

SPIEDigitalLibrary.org/conference-proceedings-of-spie

Colorectal cancer detection by hyperspectral imaging using fluorescence excitation scanning

Silas J. Leavesley, Joshua Deal, Shante Hill, Will A. Martin, Malvika Lall, et al.

Silas J. Leavesley, Joshua Deal, Shante Hill, Will A. Martin, Malvika Lall, Carmen Lopez, Paul F. Rider, Thomas C. Rich, Carole W. Boudreaux, "Colorectal cancer detection by hyperspectral imaging using fluorescence excitation scanning," Proc. SPIE 10489, Optical Biopsy XVI: Toward Real-Time Spectroscopic Imaging and Diagnosis, 104890K (19 February 2018); doi: 10.1117/12.2290696



Event: SPIE BiOS, 2018, San Francisco, California, United States

Colorectal cancer detection by hyperspectral imaging using fluorescence excitation scanning

Silas J. Leavesley^{1,2,3}, Joshua Deal^{1,2,3}, Shante Hill⁷, Will A. Martin⁴, Malvika Lall⁵, Carmen Lopez⁴, Paul F. Rider⁶, Thomas C. Rich^{2,3}, and Carole W. Boudreaux⁷

¹Department of Chemical and Biomolecular Engineering, University of South Alabama; ²Department of Pharmacology, University of South Alabama; ³Center for Lung Biology, University of South Alabama; ⁴Medical Sciences, University of South Alabama; ⁵Department of Biomedical Sciences, University of South Alabama; ⁶Department of Surgery, University of South Alabama; ⁷Department of Pathology, University of South Alabama

ABSTRACT

Hyperspectral imaging technologies have shown great promise for biomedical applications. These techniques have been especially useful for detection of molecular events and characterization of cell, tissue, and biomaterial composition. Unfortunately, hyperspectral imaging technologies have been slow to translate to clinical devices – likely due to increased cost and complexity of the technology as well as long acquisition times often required to sample a spectral image. We have demonstrated that hyperspectral imaging approaches which scan the fluorescence excitation spectrum can provide increased signal strength and faster imaging, compared to traditional emission-scanning approaches. We have also demonstrated that excitation-scanning approaches may be able to detect spectral differences between colonic adenomas and adenocarcinomas and normal mucosa in flash-frozen tissues. Here, we report feasibility results from using excitation-scanning hyperspectral imaging to screen pairs of fresh tumoral and nontumoral colorectal tissues. Tissues were imaged using a novel hyperspectral imaging fluorescence excitation scanning microscope, sampling a wavelength range of 360-550 nm, at 5 nm increments. Image data were corrected to achieve a NIST-traceable flat spectral response. Image data were then analyzed using a range of supervised and unsupervised classification approaches within ENVI software (Harris Geospatial Solutions). Supervised classification resulted in >99% accuracy for single-patient image data, but only 64% accuracy for multi-patient classification (n=9 to date), with the drop in accuracy due to increased false-positive detection rates. Hence, initial data indicate that this approach may be a viable detection approach, but that larger patient sample sizes need to be evaluated and the effects of inter-patient variability studied.

Keywords: Spectral, Spectroscopy, Signature, Fingerprint, Optical, Biopsy, Classification, EEM

1. INTRODUCTION

Spectral imaging technologies were developed in the mid-twentieth century for satellite imagery and remote sensing applications^{1,2}. These technologies were quickly expanded to the scale of acquiring hundreds of spectral data bands per image. Within the past two decades, spectral imaging technologies have been adapted to a range of biomedical imaging applications^{3–6}, and commercial systems for spectral imaging microscopy are currently available from a range of vendors. Spectral biomedical imaging has shown utility for a great range of assays, including cell identification⁷, protein quantification^{8–10}, tissue screening^{11–13}, *in vivo* animal imaging^{14,15}, and others, using either endogenous or exogenous labels. However, spectral imaging approaches have been slow to translate to clinical devices, likely due to the increased cost, instrument complexity, image acquisition times, and complexity of interpreting the multidimensional data. Despite these obstacles, tissue spectroscopy and spectral imaging contain great promise for developing next generation clinical screening devices^{16–19}.

Optical Biopsy XVI: Toward Real-Time Spectroscopic Imaging and Diagnosis, edited by Robert R. Alfano, Stavros G. Demos Proc. of SPIE Vol. 10489, 104890K · © 2018 SPIE · CCC code: 1605-7422/18/\$18 · doi: 10.1117/12.2290696

Here, we report initial results in using a new hyperspectral imaging approach that scans the fluorescence excitation spectrum for screening of colorectal tissues. While the study size is small (n=9 patients), preliminary results indicate that fluorescence excitation data may be a feasible means to discriminate tumoral and nontumoral colorectal tissue specimens. We quantitatively evaluated the ability to classify pixels from spectral images of tumoral and nontumoral specimens using a range of supervised classification algorithms, and here we report the results of applying a maximum likelihood classifier algorithm to discriminate spectral signatures. These initial results demonstrate that hyperspectral imaging technologies continue to hold great potential for tissue diagnosis and that further work must be done to translate these technologies to clinical imaging devices that are both accurate and intuitive.

2. METHODS

2.1 Sample procurement and preparation

Pairs of resected tumoral and nontumoral colorectal tissues were obtained through the University of South Alabama Departments of Surgery and Pathology, as described previously^{20,21} but using a modified protocol where fresh (nonfrozen) specimens were obtained. All specimens were obtained as residual (left over) tissues from routine standard of care surgical bowel resections and in accordance with procedures approved by the University of South Alabama Office of Research Compliance and Assurance. After resection by the Department of Surgery, tissues were separated into tumoral and nontumoral specimens by the Department of Pathology. Histology was confirmed through cryoslice, hematoxylin and eosin (H&E) stain, and microscopic examination. The remaining unfixed and unfrozen portion of tissue specimens were transported on ice for imaging.

2.2 Hyperspectral image acquisition

Fresh tissue specimens were placed on 25 mm round glass coverslip, mounted in Attofluor cell chamber (ThermoFisher Scientific), and hydrated with cold phosphate buffered saline (PBS). When appropriate, specimens were subdivided to a size that facilitated mounting and microscopic investigation. Specimens were imaged using a custom hyperspectral imaging fluorescence excitation-scanning (HIFEX) microscope system, described in part elsewhere^{22–24}. In brief, the system consisted of a 300W Xe arc lamp (Titan 300, Sunoptic Technologies), a thin-film tunable filter array (VersaChrome filters, Semrock, IDEX Health & Science, LLC), an automated inverted fluorescence microscope platform (TE2000-U, Nikon Instruments), custom long-pass dichroic filters (Semrock), and an electron-multiplied charge-coupled device camera (Rolera EM-C², QImaging). Fluorescence hyperspectral image data were acquired using an excitation wavelength range of 360-550 nm, in 5 nm increments. For each specimen, a region with no tissue was also imaged to measure any non-specific background (mixture of stray light, cross-talk, autofluorescent molecules in buffer, etc.).

2.3 Analysis approach

Spectral image datasets were corrected to a flat, NIST-traceable spectral response using previously described calibration procedures^{7,25}. In brief, the spectral response of the system was measured using a fiber-coupled high-sensitivity spectrometer (QE65000, Ocean Optics, Inc.), equipped with an integrating sphere (FOIS-1, Ocean Optics, Inc.) and calibrated to a NIST-traceable illumination source (LS-1-CAL-INT, Ocean Optics, Inc.). A wavelength-dependent intensity correction coefficient was calculated and a custom MATLAB script was used to correct the intensity of all acquired spectral images to NIST-traceable response using the correction coefficient. As part of this process, non-specific background was measured from background regions and subtracted from all sample fields of view for each specimen. Images were then converted to band-sequential (BSQ) file format using a custom MATLAB script for future analysis. Collections of spectral image data from all fields of view from a single specimen and fields of view from multiple specimens were also tiled using a custom MATLAB script.

Corrected spectral image datasets were analyzed using ENVI software (Harris Geospatial Solutions). When appropriate, regions of interest were selected and average spectra from each region were extracted. Supervised classification was performed using a range of classifiers available in ENVI, including maximum likelihood, neural network, Mahalanobis distance, and others. Classifier performance was evaluated using a range of statistical metrics, including sensitivity, specificity, accuracy, and confusion matrix.

3. RESULTS AND DISCUSSION

Hyperspectral imaging approaches may hold great promise for quantitative analysis of cells and tissues, and especially for diagnosis of a range of pathologies, including cancer. Here, we evaluated the preliminary ability of a new form of hyperspectral imaging, HIFEX, for detecting spectral differences between tumoral and nontumoral resected fresh colorectal tissue specimens. In general, hyperspectral images of tumoral and nontumoral specimens displayed marked spectral variations (Figure 1). However, spectral variations were also observed between regions within a single specimen, although visually of less magnitude than the variations between tumoral and nontumoral specimens. Hence, to quantitatively evaluate the ability to distinguish tumoral from nontumoral specimens, a range of supervised classification approaches was evaluated.

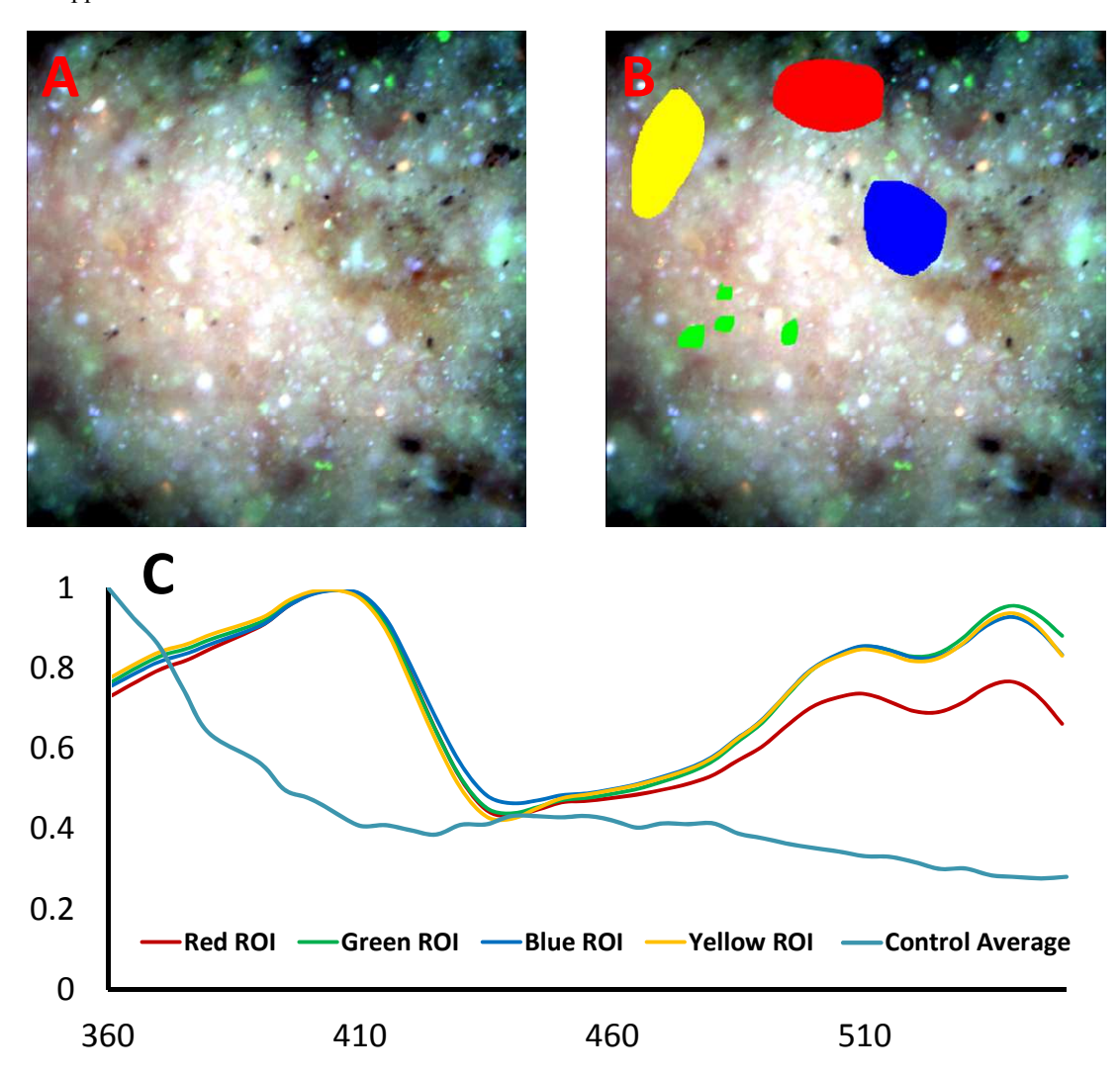


Figure 1: Example spectral image of a tumoral specimen (A) with regions of interest selected (B) to extract representative spectra (C). The average spectrum extracted from the nontumoral (control) specimen is also shown in blue.

To implement supervised classification in the ENVI software environment, spectral image data was first stitched to produce a single image containing all fields of view from each patient, including fields of view from both tumoral and nontumoral specimens (Figure 2). In addition, stitched images were also produced that contained tumoral and nontumoral fields of view from multiple patients, to investigate the effects of patient-to-patient variation on classification performance (Figure 3). Training regions corresponding to a subset of pixels were then defined within a subset of fields from tumoral and nontumoral specimens. Truth regions were also defined to indicate which regions were tumoral and which were nontumoral.

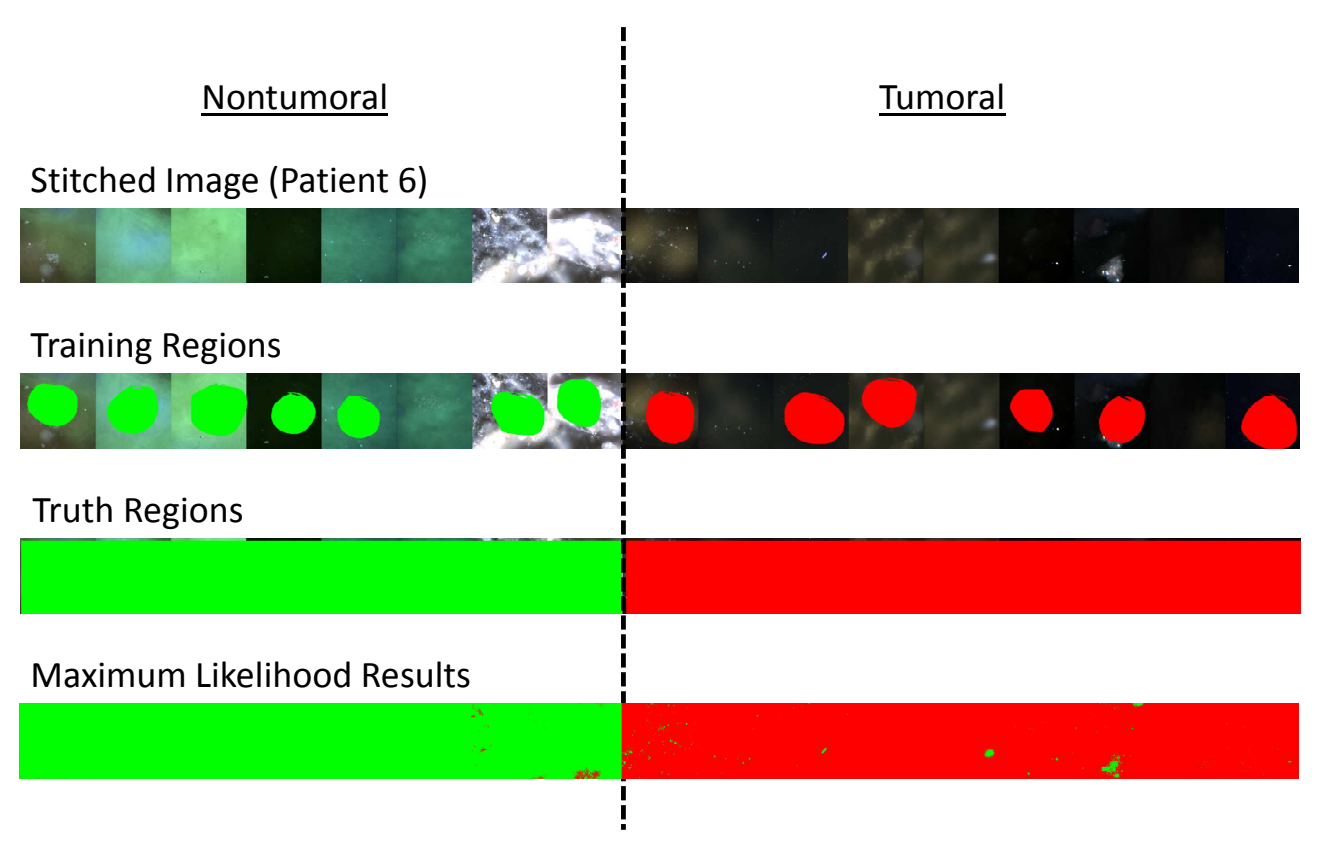


Figure 2: 1st Row) Example stitched spectral image of fields of view from patient #6. Fields of view from the nontumoral specimen are shown at left and fields of view from the tumoral specimen are shown at right. 2nd Row) Training regions were selected among a subset of the fields of view. 3rd Row) Truth regions were selected to define all tumoral and nontumoral fields of view. 4th Row) Results from maximum likelihood classification where green pixels were classified as nontumoral and red pixels were classified as tumoral.

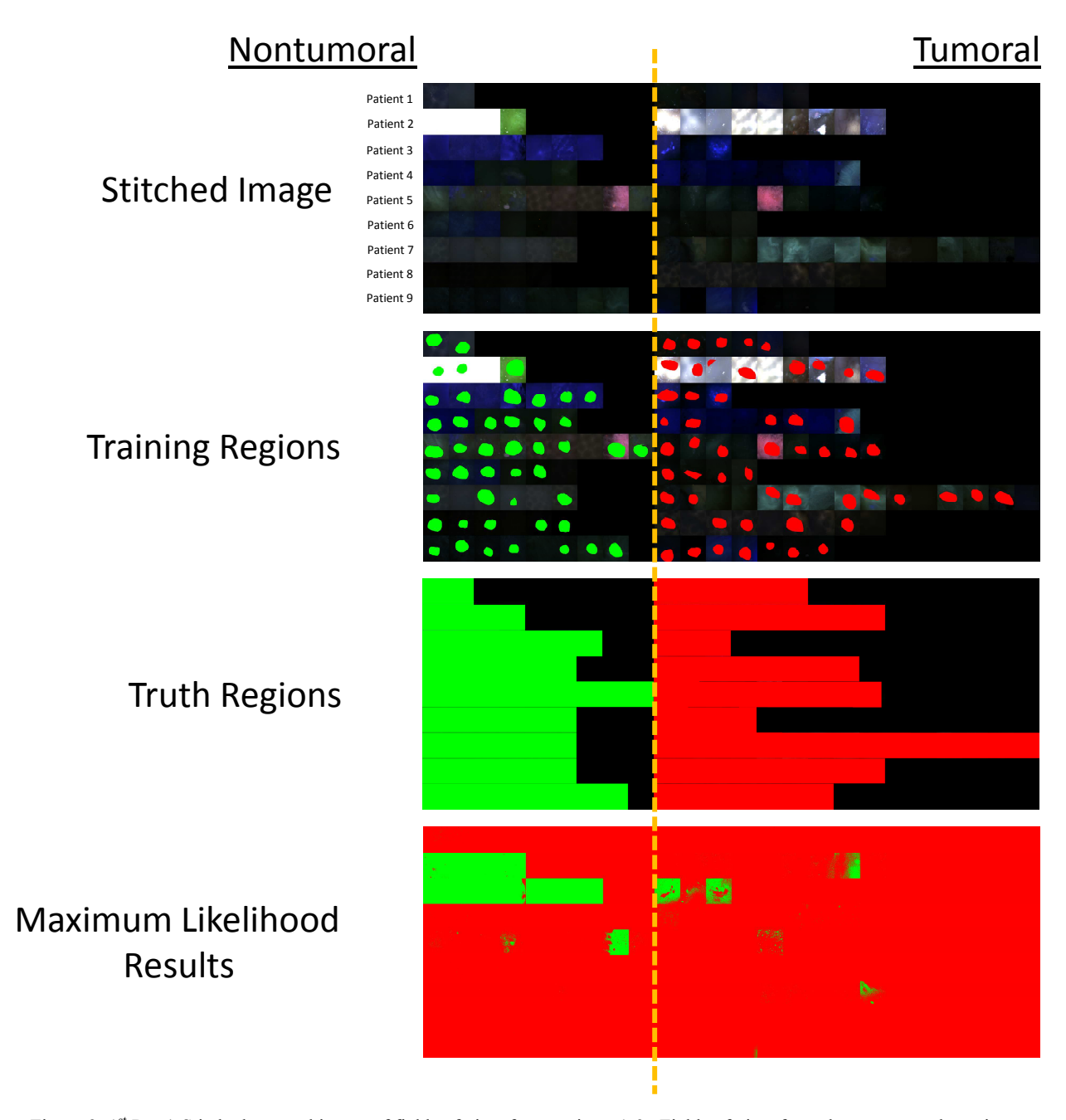


Figure 3: 1st Row) Stitched spectral image of fields of view from patients 1-9. Fields of view from the nontumoral specimen are shown at left and fields of view from the tumoral specimen are shown at right. 2nd Row) Training regions were selected among a subset of the fields of view. 3rd Row) Truth regions were selected to define all tumoral and nontumoral fields of view. 4th Row) Results from maximum likelihood classification where green pixels were classified as nontumoral and red pixels were classified as tumoral. Several fields of view can be identified as obvious outliers that were misclassified.

A range of classifiers were examined to evaluate the ability to differentiate tumoral and nontumoral specimens based on excitation spectral signatures. Results from the maximum likelihood classifier indicate that it is, in general, an effective supervised classifier for differentiating spectral images from tumoral and nontumoral colorectal tissues (Figure 4). Of note, intra-patient spectral variations were in general small, resulting in a very high classification accuracy of 99.46%. However, inter-patient spectral variations were more significant, resulting in a lower classification accuracy of 63.98%. However, even with reduced classification accuracy, it should also be noted that the confusion matrix results indicate

that 96.66% of tumoral tissues were correctly identified as tumoral, corresponding to a 96% sensitivity for correctly detecting pixels within tumoral spectral images.

Patient 6

Overall Accuracy	4126034/4148488		99.46%
Kappa Coefficient	0.9891		
	Ground Truth	(Pixels)	
Class	Benign_Truth	Lesional_Truth	Total
Benign_Training	1946989	15003	1961992
Lesional_Training	7451	2179045	2186496
Total	1954440	2194048	4148488
	Ground Truth	(Percent)	
Class	Benign_Truth	Lesional_Truth	Total
Benign_Training	99.62	0.68	47.29
Lesional_Training	0.38	99.32	52.71
Total	100	100	100

Patients 1-9

Overall Accuracy	(19824308/30986228)		63.98%
Kappa Coefficient	0.2009		
	Ground Truth	(Pixels)	
Class	Benign_Truth	Lesional_Truth	Total
Unclassified	0	0	0
Benign_Training	2940339	584151	3524490
Lesional_Training	10577769	16883969	27461738
Total	13518108	17468120	30986228
	Ground Truth	(Percent)	
Class	Benign_Truth	Lesional_Truth	Total
Unclassified	0	0	0
Benign_Training	21.75	3.34	11.37
Lesional_Training	78.25	96.66	88.63
Total	100	100	100

Figure 4: Maximum likelihood classifier results for patient #6 (left) and patients #1-9 (right), corresponding to stitched images shown in Figure 2 and Figure 3, respectively. Classification accuracy (shown in the upper right of each panel) as well as a confusion matrix showing % in each class (shown at the bottom of each panel) are the main metrics of classification performance. All metrics are presented on a pixel-wise basis.

4. CONCLUSIONS AND FUTURE WORK

Hyperspectral imaging technologies began to be adopted from the remote sensing field to biomedical microscopy and other biomedical imaging applications over 2 decades ago. However, these technologies have been slow to become translated to clinical detection devices, due to a range of factors including cost, complexity, image acquisition speed, and data complexity. Here, we show that hyperspectral image data from resected tumoral and nontumoral colorectal tissue specimens can be used with automated classification algorithms to accurately discriminate pixels in tumoral spectral images from those in nontumoral images. However, we also show that patient-to-patient variation in spectral image data is non-negligible. Hence, a potential area of future work is to investigate the nature of patient-to-patient variability in fluorescence excitation spectra of colorectal tissues and to develop classification algorithms that better account for a reasonable range of clinical variability.

5. ACKNOWLEDGEMENTS

The authors would like to acknowledge support from NIH grants P01 HL066299, UL1 TR001417, S10 RR027535, S10 OD020149, NSF grants 1725937, and the Abraham Mitchell Cancer Research Fund. The authors (Drs. Leavesley and Rich) also disclose financial interest in a start-up company, SpectraCyte LLC, formed to commercialize spectral imaging technologies.

REFERENCES

- [1] Fink, D.J., "Monitoring earth's resources from space," Technology Review 75, 32–41 (1973).
- [2] Goetz, A.F.H., Vane, G., Solomon, J.E., and Rock, B.N., "Imaging spectrometry for earth remote sensing," Science 228(4704), 1147–1152 (1985).
- [3] Garini, Y., Young, I., and McNamara, G., "Spectral imaging: principles and applications," Cytometry Part A 69(8), 735–747 (2006).
- [4] McNamara, G., Gupta, A., Reynaert, J., Coates, T.D., and Boswell, C., "Spectral imaging microscopy web sites and data," Cytometry Part A 69(8), 863–871 (2006).
- [5] Li, Q., He, X., Wang, Y., Liu, H., Xu, D., and Guo, F., "Review of spectral imaging technology in biomedical engineering: achievements and challenges," Journal of biomedical optics 18(10), 100901–100901 (2013).

- [6] Lu, G., and Fei, B., "Medical hyperspectral imaging: a review," Journal of biomedical optics 19(1), 010901–010901 (2014).
- [7] Leavesley, S.J., Annamdevula, N., Boni, J., Stocker, S., Grant, K., Troyanovsky, B., Rich, T.C., and Alvarez, D.F., "Hyperspectral imaging microscopy for identification and quantitative analysis of fluorescently-labeled cells in highly autofluorescent tissue," Journal of Biophotonics 5(1), 67–84 (2012).
- [8] Chen, Y., Mauldin, J.P., Day, R.N., and Periasamy, A., "Characterization of spectral FRET imaging microscopy for monitoring nuclear protein interactions," Journal of Microscopy 228(2), 139–152 (2007).
- [9] Leavesley, S.J., Britain, A., Cichon, L.K., Nikolaev, V.O., and Rich, T.C., "Assessing FRET using spectral techniques," Cytometry Part A 83(10), 898–912 (2013).
- [10] Levy, S., Wilms, C.D., Brumer, E., Kahn, J., Pnueli, L., Arava, Y., Eilers, J., and Gitler, D., "SpRET: Highly sensitive and reliable spectral measurement of absolute FRET efficiency," Microscopy and Microanalysis 17(02), 176–190 (2011).
- [11] Andersson-Engels, S., Johansson, J., and Svanberg, S., "Medical diagnostic system based on simultaneous multispectral fluorescence imaging," Applied Optics 33(34), 8022–8029 (1994).
- [12] Mansfield, J.R., Sowa, M.G., Payette, J.R., Abdulrauf, B., Stranc, M.F., and Mantsch, H.H., "Tissue viability by multispectral near infrared imaging: a fuzzyC-means clustering analysis," Medical Imaging, IEEE Transactions on 17(6), 1011–1018 (1998).
- [13] Farina, B., Bartoli, C., Bono, A., Colombo, A., Lualdi, M., Tragni, G., and Marchesini, R., "Multispectral imaging approach in the diagnosis of cutaneous melanoma: potentiality and limits," Physics in Medicine and Biology 45(5), 1243–1254 (2000).
- [14] Leavesley, S.J., Jiang, Y., Patsekin, V., Rajwa, B., and Robinson, J.P., "An excitation wavelength--scanning spectral imaging system for preclinical imaging," Review of Scientific Instruments 79(2), 023707–023710 (2008).
- [15] Chaudhari, A.J., Darvas, F., Bading, J.R., Moats, R.A., Conti, P.S., Smith, D.J., Cherry, S.R., and Leahy, R.M., "Hyperspectral and multispectral bioluminescence optical tomography for small animal imaging," Physics in Medicine and Biology 50(23), 5421–5441 (2005).
- [16] Alfano, R., Tata, D., Cordero, J., Tomashefsky, P., Longo, F., and Alfano, M., "Laser induced fluorescence spectroscopy from native cancerous and normal tissue," Quantum Electronics, IEEE Journal of 20(12), 1507–1511 (1984).
- [17] Bigio, I.J., and Mourant, J.R., "Ultraviolet and visible spectroscopies for tissue diagnostics: fluorescence spectroscopy and elastic-scattering spectroscopy," Physics in Medicine and Biology 42(5), 803 (1997).
- [18] Richards-Kortum, R., and Sevick-Muraca, E., "Quantitative optical spectroscopy for tissue diagnosis," Annual Reviews in Physical Chemistry 47, 555–606 (1996).
- [19] Wagnieres, G.A., Star, W.M., and Wilson, B.C., "In vivo fluorescence spectroscopy and imaging for oncological applications," Photochemistry and photobiology 68(5), 603–632 (1998).
- [20] Leavesley, S.J., Wheeler, M., Lopez, C., Baker, T., Favreau, P.F., Rich, T.C., Rider, P.F., and Boudreaux, C.W., "Hyperspectral imaging fluorescence excitation scanning for detecting colorectal cancer: pilot study," presented at SPIE BiOS, 2016, 970315–970315.
- [21] Leavesley, S.J., Walters, M., Lopez, C., Baker, T., Favreau, P.F., Rich, T.C., Rider, P.F., and Boudreaux, C.W., "Hyperspectral imaging fluorescence excitation scanning for colon cancer detection," Journal of Biomedical Optics 21(10), 104003–104003 (2016).
- [22] Favreau, P.F., Hernandez, C., Heaster, T., Alvarez, D.F., Rich, T.C., Prabhat, P., and Leavesley, S.J., "Excitation-scanning hyperspectral imaging microscope," Journal of biomedical optics 19(4), 046010–046010 (2014).
- [23] Favreau, P.F., Hernandez, C., Lindsey, A.S., Alvarez, D.F., Rich, T.C., Prabhat, P., and Leavesley, S.J., "Thin-film tunable filters for hyperspectral fluorescence microscopy," Journal of biomedical optics 19(1), 011017–011017 (2014).
- [24] Favreau, P.F., Rich, T.C., Prabhat, P., and Leavesley, S.J., "Tunable thin-film optical filters for hyperspectral microscopy," presented at SPIE BiOS, 2013, 85890R–85890R.
- [25] Annamdevula, N.S., Sweat, B., Favreau, P., Lindsey, A.S., Alvarez, D.F., Rich, T.C., and Leavesley, S.J., "An approach for characterizing and comparing hyperspectral microscopy systems," Sensors 13(7), 9267–9293 (2013).